Journal of Non-Newtonian Fluid Mechanics 167–168 (2012) 95–105

Contents lists available at SciVerse ScienceDirect

Journal of Non-Newtonian Fluid Mechanics

journal homepage: http://www.elsevier.com/locate/jnnfm

Analysis of isothermal flow of a Phan-Thien—Tanner fluid in a simplified model of a single-screw extruder

D.O.A. Cruz [a], F.T. Pinho [b,*]

[a] Departamento de Engenharia Mecânica, Universidade Federal do Pará, Campus do Guamá, 66075-900 Belém, Brazil
[b] Centro de Estudos de Fenómenos de Transporte, Faculdade de Engenharia da Universidade do Porto, Rua Dr. Roberto Frias s/n, 4200-465 Porto, Portugal

ARTICLE INFO

Article history:
Received 2 June 2011
Received in revised form 24 October 2011
Accepted 25 October 2011
Available online 10 November 2011

Keywords:
Single-screw extruder
Phan-Thien—Tanner model
Shallow channel
Characteristic curve

ABSTRACT

An analytical solution is obtained for the flow in a simplified model of the shallow single screw extruder of polymer melts described by the simplified Phan-Thien—Tanner fluid with linear kernel function. To arrive at the analytical solution in the rectangular channel, both the effects of the channel curvature and of the spanwise coordinate are neglected in the flow (shallow channel/extruder) and the fluid properties are considered to be temperature-independent. The two Couette–Poiseuille flows are coupled via the nonlinear constitutive equation and the results are presented in dimensionless form as a function of all relevant dimensionless numbers. The results show that as shear-thinning is enhanced there is a decrease in the ratio between the strengths of the main and secondary flows and in the dimensionless pressure rise through the extruder.

1. Introduction

Pressurization and pumping of highly viscous polymer melts is a fundamental step in industrial extrusion processes and one device that is able to perform this task is the screw extruder. This device is also used in the food and the animal feed processing industries. In addition to being the single most used geometry for pumping polymers in industry, the single-screw extruder is also the building block for more complex screw-type pumping devices. A description of its operation is presented in a variety of classical books on the subject, with different levels of detail, such as in Tadmor and Klein [1], Tadmor and Gogos [2], Giles et al. [3] and Rauwendaal [4]. Clearly, it has been extensively investigated for a large variety of fluids and addressing also a wide range of operational conditions.

A screw extruder performs several tasks from the moment the polymer pellets enter the hopper to the moment the polymer melt exits through the extruding die with a specific profile geometry, including melting the polymers, pressurizing and pumping, mixing the melt and finally pushing the melt through the exit die. To accomplish these tasks the shape and dimensions of the extruder vary along it. This refers to variations in the root diameter, helix pitch and angle, helix orientation (alternating the rotation for mixing purposes) or flight width as one proceeds from the feed section to the metering section through the transition section.

As schematically shown in Fig. 1, a single-screw extruder essentially consists of a helix wound around a shaft and this screw rotates inside a cylindrical barrel. The helix has an angle θ and pitch L_s (equal to the lead for a screw with a single start) and the space between the teeth defines a channel through which the polymer flows. Of interest to this work is the metering phase, where the polymer is in a completely melted state having a high viscosity, the cross section of the extruder is unchanged and the high temperature of the melt is essentially kept constant or varies only by a small amount to avoid such effects as thermal degradation of the polymer and an excessive reduction in polymer viscosity, which impacts negatively on post-processing [5]. These are conditions that are more easily approached when the screw rotates at low speed. This does not eliminate thermal effects, like viscous dissipation, but in this work the thermal energy equation is not solved and since temperature variations are kept to a minimum the fluid properties are considered to be independent of temperature.

Since the polymer melt has a high viscosity, the centrifugal forces are negligible in comparison with the viscous and pressure forces and so a Galilean transformation can be applied. Then, the fluid dynamic solution in the screw extruder, where the melt flows between the rotating screw and the stationary outer barrel, is identical to the solution of a melt flowing between a stationary screw and a rotating barrel, a transformation, which significantly simplifies the treatment of the problem. Additionally, and since the flow channel is usually thin in comparison with the radius of the shaft (shallow-screw), curvature effects are negligible and we can unwind the channel from the screw to define the simpler rectangular shallow straight channel with motion of the upper surface at an

* Corresponding author.
E-mail addresses: doac@ufpa.br (D.O.A. Cruz), fpinho@fe.up.pt (F.T. Pinho).

0377-0257/$ - see front matter © 2011 Elsevier B.V. All rights reserved.
doi:10.1016/j.jnnfm.2011.10.007

Nomenclature

Latin symbols

D_b	diameter of the barrel
D_s	diameter of the screw
e	flight width
H	thickness of the rectangular duct
L_s	helix pitch or lead
N	rotational speed of the screw [r.p.s.]
p	pressure
$p_{,x}$	imposed streamwise pressure gradient
$p_{,z}$	spanwise pressure gradient induced by plate motion
P_{zx}	ratio of pressure gradients, $p_{,z}/p_{,x}$
T_{xx}, T_{xy}, T_{yz} and T_{zz}	normalized stresses τ_{xx}, τ_{xy}, τ_{yz} and τ_{zz}, Eq. (14)
T^*_{xx}, T^*_{xy}, T^*_{yz} and T^*_{zz}	normalized stresses τ_{xx}, τ_{xy}, τ_{yz} and τ_{zz}, Eq. (23)
U_z	spanwise bulk velocity of Newtonian fluid of viscosity η under the same pressure gradient, $-p_{,z}H^2/(12\eta)$
V_p	velocity of the upper plate of the rectangular duct
V_{px}	streamwise component of the velocity of the upper plate of the rectangular duct
V_{pz}	spanwise component of the velocity of the upper plate of the rectangular duct
w	spanwise velocity component
w^*	normalized spanwise velocity component, w/U_N
W	width of the rectangular duct
$\overline{W}$	bulk velocity in the spanwise direction, $\overline{W}=0$
Wi	Weissenberg number, $\lambda U_N/H$
Wi_p	Weissenberg number, $\lambda V_p/H$
W_m	positive bulk mean velocity in spanwise direction, $W_m=\int_0^{y@w=0} w dy/H$
$\dot{W}$	pumping power
$\dot{W}^*$	pumping power normalized by Newtonian bulk velocity, Eq. (22)
$\dot{W}^*_m$	pumping power normalized by steamwise bulk velocity of PTT fluid, $\dot{W}^*_m=\dot{W}^*\left(U_N^2/U_m^2\right)$
T_{xy_0}	normalized τ_{xy} stress at lower channel wall, Eq. (14)
$T^*_{xy_0}$	normalized τ_{xy} stress at lower channel wall, Eq. (23)
T_{yz_0}	normalized τ_{yz} stress at lower channel wall, Eq. (14)
$T^*_{yz_0}$	normalized τ_{yz} stress at lower channel wall, Eq. (23)
u	streamwise velocity component
u^*	normalized streamwise velocity, u/U_N
U_m	streamwise bulk velocity of PTT fluid
U_N	streamwise bulk velocity of Newtonian fluid of viscosity η under the same pressure gradient, $-p_{,x}H^2/(12\eta)$
x	streamwise coordinate
y	transverse coordinate
y^*	normalized transverse coordinate, y/H
z	spanwise coordinate

Greek symbols

δ_f	clearance between the tip of the flight and the inner surface of the barrel
ε	extensional coefficient of the PTT fluid model
η	viscosity coefficient of the PTT fluid model
λ	relaxation time of the PTT fluid model
θ	helix angle
ρ	fluid density
τ_{xx}	xx component of the fluid extra stress tensor (streamwise normal stress)
τ_{xy}	xy component of the fluid extra stress tensor (xy shear stress)
τ_{zz}	zz component of the fluid extra stress tensor (spanwise normal stress)
τ_{zy}	zy component of the fluid extra stress tensor (zy shear stress)
ω	angular speed of the screw

angle relative to the channel longitudinal direction, as depicted in Fig. 2.

The solution of the steady fully-developed flow of a Newtonian viscous fluid in this channel is classical and is the linear sum of two Couette–Poiseuille flows, one of which is in a rectangular channel, where the corresponding streamwise velocity depends only on the transverse and spanwise coordinates, $u(y,z)$. From a general point of view any combination of Couette and Poiseuille flows is possible in a variety of applications, but in the context of the pumping action of a screw extruder what matters is the case, where the flow is essentially created by the motion of the plate (rotation of the screw) and the streamwise pressure gradient is adverse in order to pressurize the melt prior to its flow through the exit die. According to Shah and London [6] the Newtonian flow in a rectangular cross-section duct with four stationary walls was obtained by Dryden et al. [7] and Marco and Han [8]. An analytical solution for the Newtonian flow driven by the upper plate in the absence of a pressure gradient was presented by Theofilis et al. [9], who were concerned with flow instabilities. The solution of the fully-developed Couette–Poiseuille flow of a Newtonian fluid in a thin channel is straight-forward and is often a case presented in textbooks [10]. The two solutions are solved separately and combined linearly to arrive at the solution for the screw extruder flow given the linear nature of both the Newtonian fluid constitutive equation and of the momentum equation for fully-developed flow. The resulting solution is presented in various reference books [1–5].

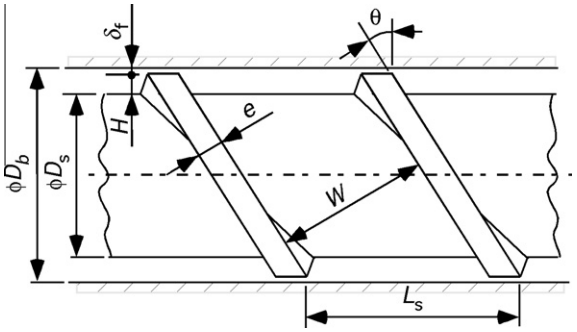

Fig. 1. Basic geometry of a single screw extruder (adapted from Fig. 6.7 of Tadmor and Gogos [2]).

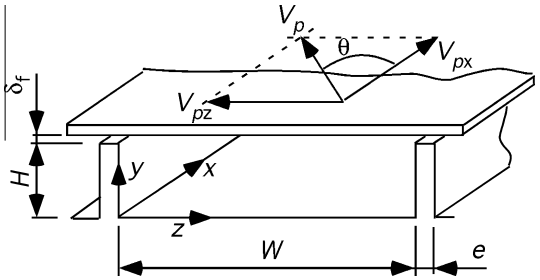

Fig. 2. Schematic representation of the flow geometry and coordinate system (adapted from Fig. 6.9 Tadmor and Gogos [2]).

According to Li and Hsieh [11], this simplified Newtonian solution is not an accurate solution for Newtonian flows except in the limit of very shallow channels ($H/D_b \leqslant 0.025$), as was also demonstrated by several experimental sets of results [12,13], but nevertheless remains a good first approximation. The discrepancies are associated with the lack of dependence of the velocity boundary conditions on the transverse coordinate after the application of the Galilean transformation. Due consideration of such variation was taken in the analytical investigation of Li and Hsieh [11] by studying the flow without such transformation.

Polymer melts are shear-thinning viscoelastic fluids that can be described by one of many complex constitutive equations such as the Phan-Thien—Tanner (PTT) model [14] used here, the Giesekus model [15], the Leonov model [16], the pom–pom model [17] or others [18] in single and multimode variants. These equations are complex and preclude a complete analytical solution in the full geometry, but are to be preferred to describe the rheology of melts since they also have the capability to predict other features that the more often used Newtonian and power law models cannot predict, such as the occurrence of secondary flows in non-circular channels or normal stress effects, among others. Gradients of normal stresses in non-circular ducts give rise to secondary flows [19] and these can actually be quite relevant in some cases as for laminar heat transfer enhancement [20,21]. More recently, Yue et al. [22] extensively reviewed the subject and proposes a criterion to identify the direction of the secondary flow based on work carried out with the Giesekus model. However, due consideration of these effects requires a numerical solution which is not carried out here.

Flow solutions for these constitutive equations can be obtained numerically and that can include also other physical phenomena such as the melting and heat transfer processes. Even though numerical computations always allow the solution of complex problems, they lack the generality of an analytical solution, which is more efficient at guiding the design and developing design concepts for engineering systems provided the underlying simplified physical conditions are met and are realistically acceptable. Of course, such an analytical solution often cannot be obtained due to the complexity of the problem in which case the designer must rely entirely on numerical solutions aided by experience or based simply on experience and trial-and-error. In any case, in the future the use of viscoelastic constitutive equations will become more common in the design of extruders both for design guidelines as well as for detailed design and an analytical solution will be helpful for this purpose.

Since rheological models for viscoelastic polymer melts are non-linear, analytical solutions are extremely difficult and researchers have alternatively tried to isolate relevant properties in an attempt to simplify the physical problem. The single-most important fluid property is the viscosity and there are solutions for the flow of shear-thinning power law fluids in a screw extruder. Poon [23] and more recently Gabriele et al. [24] solved numerically the equations considering the pressure gradient driven flow of power-law fluids to depend only on one transverse coordinate. In spite of this simplification, the simplified governing equations for the two simpler Couette–Poiseuille flows could not be solved analytically and a numerical method was required. However, for a particular condition called the close discharge operation, which is found in the helical barrel rheometer, Guzmán and Schieber [25] were able to obtain a closed analytical solution relating extrusion parameters and rheological properties of power law fluids after a suitable coordinate transformation.

To our best knowledge there are no analytical solutions for the flow of polymer melts described by quasi-linear and non-linear viscoelastic constitutive equations in a single screw extruder. Actually, and in spite of the more complex mathematical formulation of the Phan-Thien—Tanner (PTT) model vis-à-vis the power law model, an analytical solution for the open discharge problem is possible without the need for any coordinate transformation provided the linear form of the simplified PTT equation is used and the flow is assumed to depend only on a single transverse coordinate, as in the shallow single-screw extruder under the classical approach with the Galilean transformation. The derivation of the solution of this viscometric skew rectilinear flow for the PTT model and the corresponding analysis of its flow characteristics are the objective of this work. This is carried out here in a general framework, so that the results can be of use to any application, including also the specific situation of pumping in a single screw extruder. To this end we have also written in the appendix the main equations of the solution in a more explicit form for extrusion pumping, i.e., normalized by the plate velocity, which is proportional to the screw rotation.

The next section presents the flow geometry and the governing equations and is followed by the definition of all relevant non-dimensional quantities and the presentation of the normalized equations. Then, the solution is presented and results are discussed prior to a summary of the main conclusions.

2. Flow geometry and governing equations

2.1. Flow geometry

The flow geometry is that of Fig. 2 with a rectangular duct of thickness H and width W. There is a small clearance δ_f between the tip of the flight of the screw and the inner surface of the barrel of diameter D_b (D_b is shown in Fig. 1), which is of the order of 0.1–0.3% of D_b [2]. This gap is filled with polymer to lubricate and avoid metal to metal contact, but here this effect is neglected. We consider the general case, where the helix angle θ (the angle between the flight and the plane normal to the axis) can vary, although most results in Section 3 pertain to the common square-pitched screw, where the lead L_s equals the screw diameter D_s and $\theta = 17.65°$. The helix angle is related to the lead L_s (the axial distance corresponding to one full turn of the screw) and diameter via Eq. (1) showing that it varies with the position, i.e., it is larger at the root of the flight than at its tip.

$$\tan\theta = \frac{L_s}{\pi D}. \tag{1}$$

The width of the channel W is related to the lead via equation (2), where e is the flight width.

$$W = L_s\cos\theta - e. \tag{2}$$

The coordinate system is also represented in Fig. 2; x is the streamwise direction, y is the direction along the thickness and z is the direction along the width.

The motion of the upper plate depends on the angular speed ω of the screw and the radius of the screw tip (rather than the radius of the barrel [11]) and the decomposition of the velocity into its x and z components depends also on the helix angle through Eqs. (3) and (4).

$$V_p = \omega\frac{D_s + 2H}{2} = \pi N(D_s + 2H), \tag{3}$$

$$V_{px} = V_p\cos\theta \quad \text{and} \quad V_{pz} = V_p\sin\theta, \tag{4}$$

where N is the rotational speed of the screw in [r.p.s]. The motion of the plate in the x direction together with the imposed streamwise pressure gradient moves the fluid along the rectangular channel, whereas the motion of the plate in the z direction affects mixing in the cross section. The dependence of mixing on this motion and on the other relevant quantities is a complex issue, which is not addressed here, but its quantification requires the dynamic

solution of the skew-symmetric flow obtained here as explained by Chella and Ottino [26].

2.2. Governing equations

Since we are considering an isothermal flow the equations to be solved are the continuity equation, the momentum equation and the rheological constitutive equation. In tensor notation the momentum equation for incompressible liquids is

$$\nabla \cdot \mathbf{u} = 0, \tag{5}$$

where $\mathbf{u}$ is the velocity vector, the momentum equation is

$$\rho \frac{D\mathbf{u}}{Dt} = -\nabla p + \rho \mathbf{g} + \nabla \cdot \boldsymbol{\tau}, \tag{6}$$

where ρ is the fluid density, p is the pressure, $\mathbf{g}$ is the acceleration of gravity vector, D/Dt is the material derivative and $\boldsymbol{\tau}$ is the fluid extra stress tensor. This stress is described by the rheological constitutive equation, which for the linear form of the simplified Phan-Thien–Tanner model is given by

$$f(tr\ \boldsymbol{\tau})\boldsymbol{\tau} + \lambda \overset{\nabla}{\boldsymbol{\tau}} = 2\eta \mathbf{D}. \tag{7}$$

In Eq. (3) λ is the relaxation time of the fluid, η is the viscosity coefficient of the model and $\overset{\nabla}{\boldsymbol{\tau}}$ denotes the upper convected derivative of the stress given by

$$\overset{\nabla}{\boldsymbol{\tau}} = \frac{D\boldsymbol{\tau}}{Dt} - \boldsymbol{\tau} \cdot \nabla \mathbf{u} - \nabla \mathbf{u}^T \cdot \boldsymbol{\tau}. \tag{8}$$

The function of the trace in Eq. (7) is the linearized form of the exponential function (cf. Phan-Thien and Tanner [14]) and is given by

$$f(tr\boldsymbol{\tau}) = 1 + \frac{\varepsilon\lambda}{\eta} tr\boldsymbol{\tau}, \tag{9}$$

where ε is a model coefficient, which is inversely proportional to the extensional viscosity.

We will consider steady fully-developed flow in both flow directions (x and z) and that the flow only depends on the transverse coordinate y, i.e., we neglect the effect of the spanwise coordinate as in a shallow channel. This last simplifying assumption is required since for the PTT model an analytical solution is only possible if we consider the two fluid velocity components u and w to depend only on the transverse coordinate. Invoking these conditions the momentum equation, written now in index notation, becomes

$$-\frac{\partial p}{\partial x} + \frac{d\tau_{xy}}{dy} = 0 \quad \text{and} \quad -\frac{\partial p}{\partial z} + \frac{d\tau_{zy}}{dy} = 0, \tag{10}$$

and the rheological constitutive equation gives the stress components via

$$\begin{aligned}
&\left(1 + \frac{\varepsilon\lambda}{\eta}\tau_{kk}\right)\tau_{xx} = 2\lambda\tau_{xy}\frac{du}{dy},\\
&\left(1 + \frac{\varepsilon\lambda}{\eta}\tau_{kk}\right)\tau_{zz} = 2\lambda\tau_{zy}\frac{dw}{dy},\\
&\left(1 + \frac{\varepsilon\lambda}{\eta}\tau_{kk}\right)\tau_{xy} = \eta\frac{du}{dy},\\
&\left(1 + \frac{\varepsilon\lambda}{\eta}\tau_{kk}\right)\tau_{zy} = \eta\frac{dw}{dy}.
\end{aligned} \tag{11a, b, c, d}$$

Note that, whereas the pressure gradient $p_{,x} = \partial p/\partial x$ is imposed, the pressure gradient $p_{,z} = \partial p/\partial z$ is set by the condition of null flow rate in the secondary flow direction, i.e., by Eq. (12)

$$\overline{W} = \frac{1}{H}\int_0^H w dy = 0, \tag{12}$$

which needs to be solved in addition to Eqs. (10) and (11) to provide $p_{,z}$.

The analytical solution will be made non-dimensional by a suitable choice of characteristic length and velocity scales and there are at least two choices to consider: (1) a set of scales for the general solution of the skew-symmetric flow or (2) a set of scales that is more appropriate for the screw extruder. We opt for the first set in the main text, but we also provide the second set in the appendix, together with the corresponding solution equations and rules of transformation. The two sets only differ in the velocity scale, from which several dimensionless numbers are built, but this is enough to modify significantly the complex mathematical solution. In both cases the characteristic length scale is H (cf. Fig. 2). For the general solution the characteristic velocity scale is U_N, the streamwise bulk velocity for a Newtonian fluid of identical viscosity coefficient η under the same streamwise pressure gradient $p_{,x}$, which is given by

$$U_N = -\frac{p_{,x}H^2}{12\eta}. \tag{13}$$

The dimensionless solution depends on the transverse dimensionless coordinate y/H, the helix angle θ, the Weissenberg number $Wi = \lambda U_N/H$, the PTT model coefficient ε and the ratio V_p/U_N between the barrel/plate velocity (V_p) and the characteristic velocity scale. Stresses will be normalized as in

$$T_{ij} = \frac{\tau_{ij}}{6\eta U_N/H}, \tag{14}$$

and for compactness the ratio of pressure gradients $P_{zx} = \frac{p_{,z}}{p_{,x}}$ will be used.

For the extruder oriented solution presented in Appendix A, the characteristic velocity is V_p.

3. Analytical solution

Initially, the relevant governing equations are normalized in accordance to the selected scales. Then, from the rheological constitutive equations, dividing Eq. (11-a) by Eq. (11-c) and dividing Eq. (11-b) by Eq. (11-d) we find the following two relationships between the normal and shear stresses

$$\begin{aligned}
T_{xx} &= 12WiT_{xy}^2,\\
T_{zz} &= 12WiT_{zy}^2.
\end{aligned} \tag{15-a, b}$$

These are used together with the normalized forms of Eqs. (11-c) and (11-d)

$$\begin{aligned}
\frac{du^*}{dy^*} &= 6T_{xy}[1 + 6\varepsilon Wi(T_{xx} + T_{zz})],\\
\frac{dw^*}{dy^*} &= 6T_{zy}[1 + 6\varepsilon Wi(T_{xx} + T_{zz})],
\end{aligned} \tag{16-a, b}$$

where $u^* = u/U_N$ and $y^* = y/H$.

Back-substituting Eqs. (15-a) and (15-b) into Eqs. (16-a) and (16-b) gives

$$\begin{aligned}
\frac{du^*}{dy^*} &= 6T_{xy}\left[1 + 72\varepsilon Wi^2\left(T_{xy}^2 + T_{zy}^2\right)\right],\\
\frac{dw^*}{dy^*} &= 6T_{zy}\left[1 + 72\varepsilon Wi^2\left(T_{xy}^2 + T_{zy}^2\right)\right],
\end{aligned} \tag{17-a, b}$$

The momentum equations are also normalized and integrated once with the stress boundary conditions $T_{xy} = T_{xy_0}$ and $T_{zy} = T_{zy_0}$ at $y = 0$ resulting in the following two expressions for the shear stress components

$$\begin{aligned}
T_{xy} &= -2\frac{y}{H} + T_{xy_0},\\
T_{zy} &= -2\frac{y}{H}P_{zx} + T_{zy_0}.
\end{aligned} \tag{18-a, b}$$

These two stress boundary conditions (T_{xy_0} and T_{zy_0}) are later related to the known velocity boundary conditions at the top wall ($y^* = 1$).

Back substituting Eqs. (18-a) and (18-b) into Eqs. (17-a) and (17-b) leads to a system of two ordinary differential equations, which were solved by Mathematica v. 5 from Wolfram Research.

After application of the velocity boundary conditions $u_{y=0} = 0$ and $w_{y=0} = 0$ the final solutions for the velocity components are given by

$$\begin{aligned}\frac{u}{U_N} &= -6\frac{y}{H}\left\{48\varepsilon Wi^2 P_{zx}^2\left(\frac{y}{H}\right)^2\left[3\frac{y}{H}-2T_{xy_0}\right]\right.\\ &\quad -48\varepsilon Wi^2 P_{zx}\frac{y}{H}\left[4\frac{y}{H}-3T_{xy_0}\right]T_{zy_0}\\ &\quad +\left[\frac{y}{H}-T_{xy_0}\right]\left[1+144\varepsilon Wi^2\left(\frac{y}{H}\right)^2\right.\\ &\quad \left.\left.+72\varepsilon Wi^2\left[-2\frac{y}{H}T_{xy_0}+T_{xy_0}^2+T_{zy_0}^2\right]\right]\right\},\\ \frac{w}{U_N} &= -6\frac{y}{H}\left\{144\varepsilon Wi^2 P_{zx}\left(\frac{y}{H}\right)^3\left[1+P_{zx}^2\right]\right.\\ &\quad -96\varepsilon Wi^2\left(\frac{y}{H}\right)^2\left[2P_{zx}T_{xy_0}+T_{zy_0}+3P_{zx}^3T_{zy_0}\right]\\ &\quad -T_{zy_0}\left[1+72\varepsilon Wi^2\left(T_{xy_0}^2+T_{zy_0}^2\right)\right]\\ &\quad \left.+\frac{y}{H}\left[144\varepsilon Wi^2T_{xy_0}T_{zy_0}+P_{zx}\left[1+72\varepsilon Wi^2\left(T_{xy_0}^2+3T_{zy_0}^2\right)\right]\right]\right\}.\end{aligned} \tag{19-a, b}$$

Application of the velocity boundary conditions at the top wall ($u/U_N = V_p/U_N \times \cos\theta$ and $w/U_N = V_p/U_N \times \sin\theta$ at $y/H = 1$) provides the wall shear stresses T_{xy_0} and T_{zy_0} and the condition of null flow rate in the z-direction ($\overline{W} = 0$) quantifies the corresponding pressure gradient ($p_{,z}$) via its normalized form P_{zx}. However, these three quantities are not given as explicit expressions, but must be calculated numerically from the following set of three nonlinear algebraic equations

$$\begin{aligned}&-6\left\{48\varepsilon Wi^2P_{zx}^2(3-2T_{zy_0})-48\varepsilon Wi^2P_{zx}T_{zy_0}(4-3T_{xy_0})+(1-T_{xy_0})\right.\\ &\left.\times\left[1+144\varepsilon Wi^2+72\varepsilon Wi^2\left(T_{xy_0}^2-2T_{xy_0}+T_{zy_0}^2\right)\right]\right\}=\frac{V_p}{U_N}\cos\theta\end{aligned} \tag{20-a}$$

$$\begin{aligned}&-6\left\{144\varepsilon Wi^2P_{zx}\left(1+P_{zx}^2\right)+144\varepsilon Wi^2T_{xy_0}T_{zy_0}\right.\\ &-96\varepsilon Wi^2\left(2P_{zx}T_{xy_0}+T_{zy_0}+3P_{zx}^2T_{zy_0}\right)\\ &-T_{zy_0}\left[1+72\varepsilon Wi^2\left(T_{xy_0}^2+T_{zy_0}^2\right)\right]\\ &\left.+P_{zx}\left[1+72\varepsilon Wi^2\left(T_{xy_0}^2+3T_{zy_0}^2\right)\right]\right\}=\frac{V_p}{U_N}\sin\theta\end{aligned} \tag{20-b}$$

$$\begin{aligned}&-\frac{2}{5}P_{zx}\left\{5+432\varepsilon Wi^2+72\varepsilon Wi^2\left[6P_{zx}^2+5T_{xy_0}(T_{xy_0}-2)\right]\right\}\\ &+3T_{zy_0}+72\varepsilon Wi^2T_{zy_0}\left[2+6P_{zx}^2+T_{xy_0}(3T_{xy_0}-4)\right]\\ &+216\varepsilon Wi^2T_{zy_0}^2(T_{zy_0}-2)=0.\end{aligned} \tag{20-c}$$

For each set of applied conditions, namely H, θ, V_p and $p_{,x}$ and fluid properties λ, η and ε, all the independent dimensionless numbers are calculated and then the system of Eqs. (20) is numerically solved to obtain the numerical values of T_{xy_0}, T_{zy_0} and P_{zx} required to determine the velocity profiles and other quantities discussed below. The numerical solution of the system of algebraic Eqs. (20) was also carried out using Mathematica v5 from Wolfram Research.

Integration of the streamwise velocity profile provides the bulk velocity U_m given in normalized form as

$$\begin{aligned}\frac{U_m}{U_N} &= -2-\frac{864\varepsilon Wi^2}{5}+3T_{xy_0}+\frac{72}{5}\varepsilon Wi^2\left\{2P_{zx}^2(5T_{xy_0}-6)\right.\\ &\quad \left.-20P_{zx}(T_{xy_0}-1)T_{zy_0}-10T_{zy_0}^2+15T_{xy_0}\left[2+(T_{xy_0}-2)T_{xy_0}+T_{xy_0}^2\right]\right\}.\end{aligned} \tag{21}$$

The power dissipated per unit area by friction ($\dot{W}/(WL)$) is given in dimensionless form in Eq. (22)

$$\begin{aligned}\dot{W}^* &= \frac{\dot{W}/(WL)}{\eta U_N^2/H}\\ &= 12\frac{U_m}{U_N}+\frac{V_p}{U_N}\left[\cos\theta(2-T_{xy_0})+\sin\theta(-2P_{zx}+T_{zy_0})\right],\end{aligned} \tag{22}$$

where the first term on the right-hand-side is the contribution from the streamwise pressure gradient, the second term is associated with the motion of the plate in the x-direction and the last term is the contribution from the secondary flow created by the motion of the plate in the z-direction.

To analyse the pumping action of the extruder (operation under adverse streamwise pressure gradient) two quantities are of interest, but for convenience this requires the introduction of a different velocity scale. Indeed, in this context it is important to determine explicitly the flow rate as a function of the pressure inside the extruder, so the plate velocity V_p is preferred to the use of U_N in all normalizations. Hence, an alternative Weissenberg number is now defined as $Wi_p = \lambda V_p/H$, the stresses will be normalized with V_p as

$$T_{ij}^* = \frac{\tau_{ij}}{6\eta V_p/H}, \tag{23}$$

and instead of using the pressure gradient ratio, the pressure gradients are quantified and made dimensionless as follows: the dimensionless streamwise gradient is given by U_N/V_p and the dimensionless spanwise gradient is quantified as the velocity ratio U_z/V_p, where $U_z = -p_{,z}H^2/(12\eta)$.

The maximum admissible bulk velocity ($U_{m_{\max}}$) corresponding to a null value of $p_{,x}$ is the mean velocity of the flow driven exclusively by the motion of the upper plate and is given by

$$\begin{aligned}\frac{(U_N)_{\max}}{V_p} &= \frac{1}{72}\left\{60T_{xy_0}^*\right.\\ &\quad +\frac{10^{2/3}\left(360\varepsilon Wi_p^2T_{xy_0}^{*2}+\beta_1\right)}{\left[18\varepsilon^2Wi_p^4\left(1200\varepsilon Wi_p^2T_{xy_0}^{*3}+6\beta_0+5\beta_1T_{xy_0}^*\right)+\sqrt{\beta_2}\right]^{1/3}}\\ &\quad \left.+\frac{10^{2/3}}{\varepsilon Wi_p^2}\left[18\varepsilon^2Wi_p^4\left(1200\varepsilon Wi_p^2T_{xy_0}^{*3}+6\beta_0+5\beta_1T_{xy_0}^*\right)+\sqrt{\beta_2}\right]^{1/3}\right\}\end{aligned} \tag{25}$$

where

$$\begin{aligned}\beta_0 &= 3T_{xy_0}^*\left\{1+24\varepsilon Wi_p^2\left[2\left(\frac{U_z}{V_p}\right)^2+3T_{xy_0}^{*2}+T_{zy_0}^*\left(-4\frac{U_z}{V_p}+3T_{zy_0}^*\right)\right]\right\},\\ \beta_1 &= -2-144\varepsilon Wi_p^2\left[\frac{6}{5}\left(\frac{U_z}{V_p}\right)^2+3T_{xy_0}^{*2}+T_{zy_0}^*\left(-2\frac{U_z}{V_p}+T_{zy_0}^*\right)\right],\\ \beta_2 &= 2\varepsilon^3Wi_p^6\left\{5832\varepsilon Wi_p^2\beta_0\left(400\varepsilon Wi_p^2T_{xy_0}^{*3}+\beta_0\right)\right.\\ &\quad \left.+5\beta_1\left[54\varepsilon Wi_p^2T_{xy_0}^*\left(36\beta_0-5T_{xy_0}^*\right)-\beta_1^2\right]\right\}.\end{aligned} \tag{26 a-c}$$

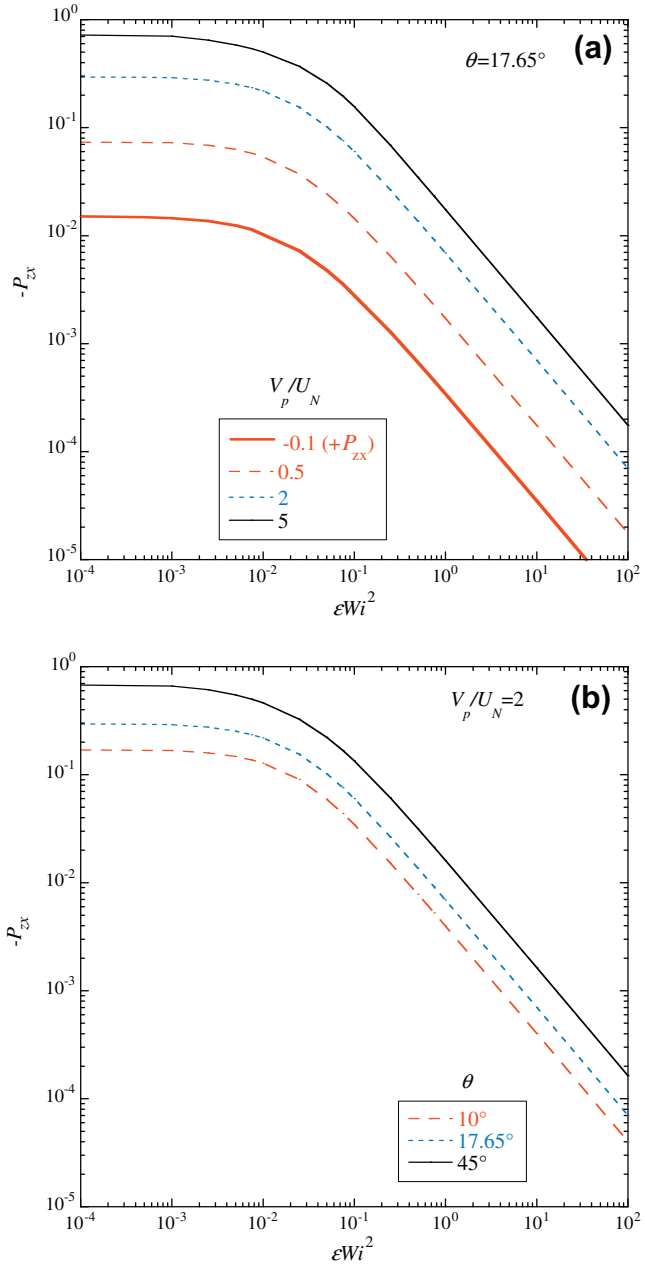

Fig. 3. Variation of $-P_{zx}$ with εWi^2: (a) fixed $\theta = 17.65°$ and as a function of V_p/U_N; (b) fixed $V_p/U_N = 2$ and as a function of θ.

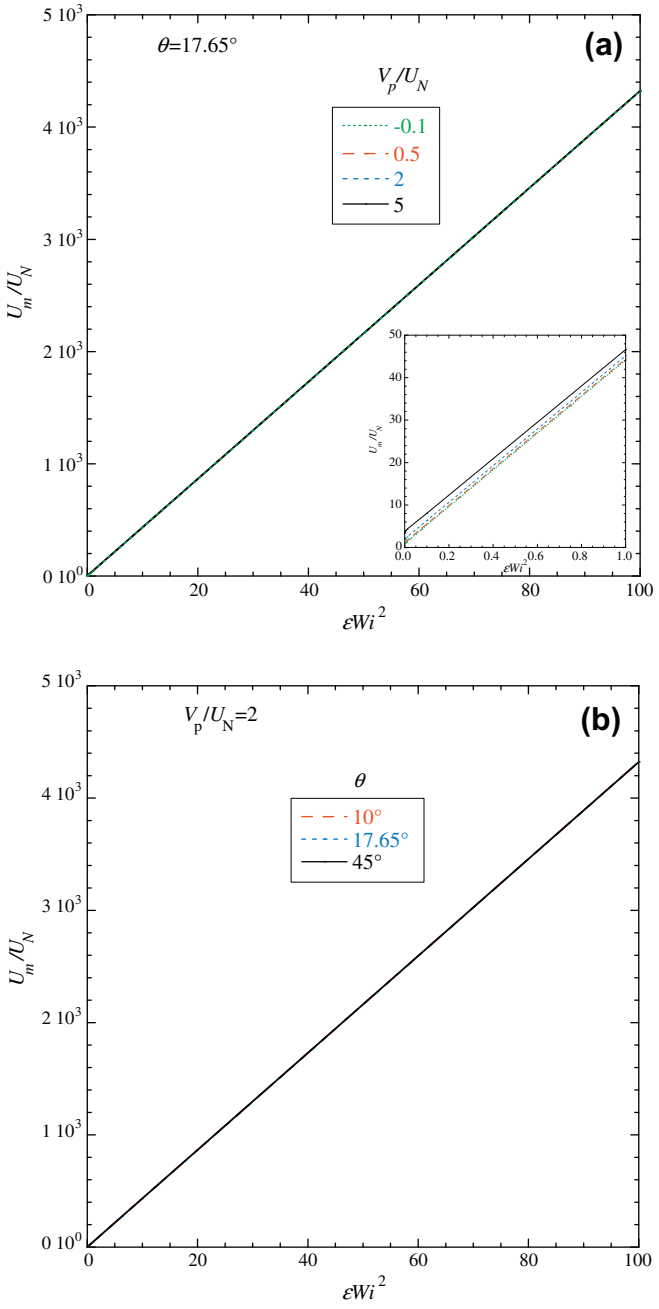

Fig. 4. Variation of U_m/U_N with εWi^2: (a) fixed $\theta = 17.65°$ and as a function of V_p/U_N; (b) fixed $V_p/U_N = 2$ and as a function of θ.

4. Results and discussion

In this section we discuss the effects of several quantities upon the velocity field, the ratio of pressure gradients and the power. The independent relevant dimensionless quantities are the screw angle θ, the magnitude of nonlinear effects of the PTT model quantified by the combination εWi^2 and the ratio V_p/U_N between the plate velocity and the velocity scale of the pressure gradient. It is important to remember at this stage that the flow in the main direction (x) is driven by the plate motion as well as by the pressure gradient $\partial p/\partial x$, whereas the motion in the secondary direction (z) is driven only by the upper plate motion and the corresponding pressure gradient $\partial p/\partial z$ is a consequence of the screw teeth stopping the flow normal to it, thus imposing a null flow rate in the z-direction.

We start by looking at Fig. 3a) to the variation of the ratio of pressure gradients $-P_{zx}$ with εWi^2 for a square screw ($\theta = 17.65°$), with V_p/U_N as a parameter. For Newtonian and weakly viscoelastic PTT fluids $-P_{zx}$ is fairly constant and weakly dependent of εWi^2 taking values of order 0.1 to 1. On further increasing εWi^2, $-P_{zx}$ changes from a plateau to a region of power law variation of type $-P_{zx} \propto 1/\varepsilon Wi^2$ (at high values of εWi^2 there is a linear variation of $-P_{zx}$ with εWi^2 with slope -1 on a log–log scale). There is here a very significant decrease of $-P_{zx}$, which reaches values of the order of 10^{-5}. It is important to remember the meaning of U_N as the bulk velocity in the main flow direction (x) for a Newtonian fluid with a viscosity equal to the zero shear rate viscosity of the PTT fluid under the action of the same pressure gradient. The ratio $-P_{zx}$ increases with V_p/U_N, because the fluid velocities in the secondary

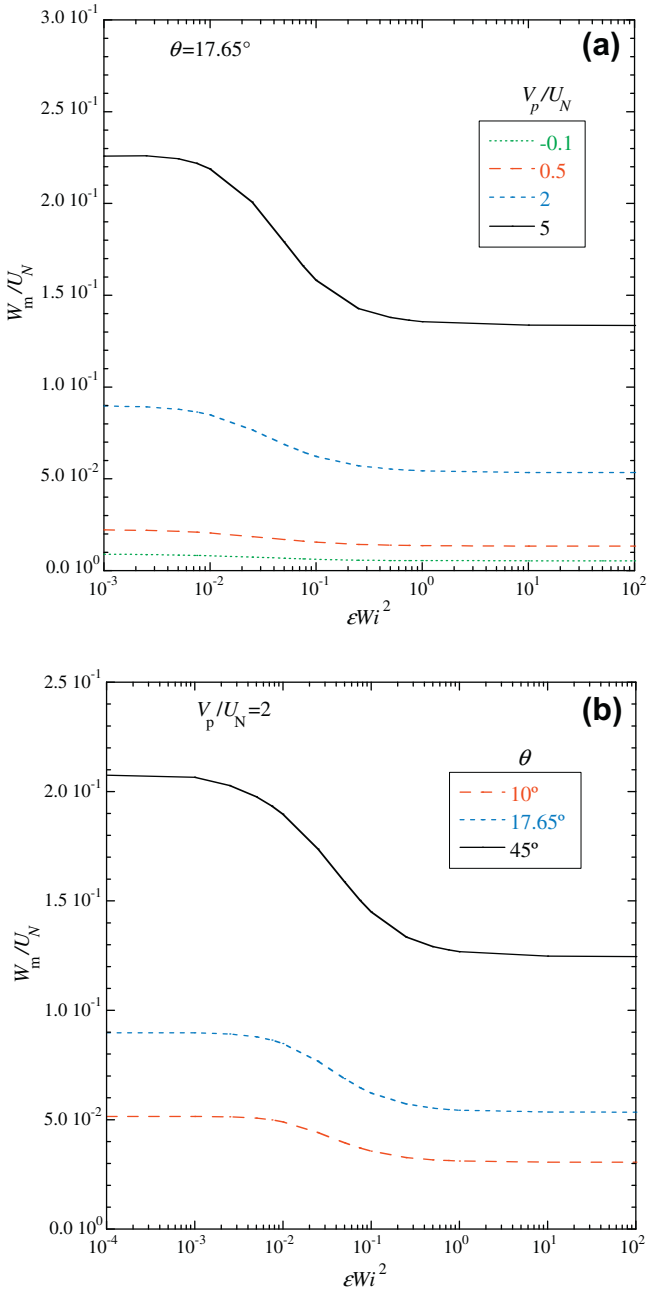

Fig. 5. Variation of W_m/U_N with εWi^2: (a) fixed $\theta = 17.65°$ and as a function of V_p/U_N; (b) fixed $V_p/U_N = 2$ and as a function of θ.

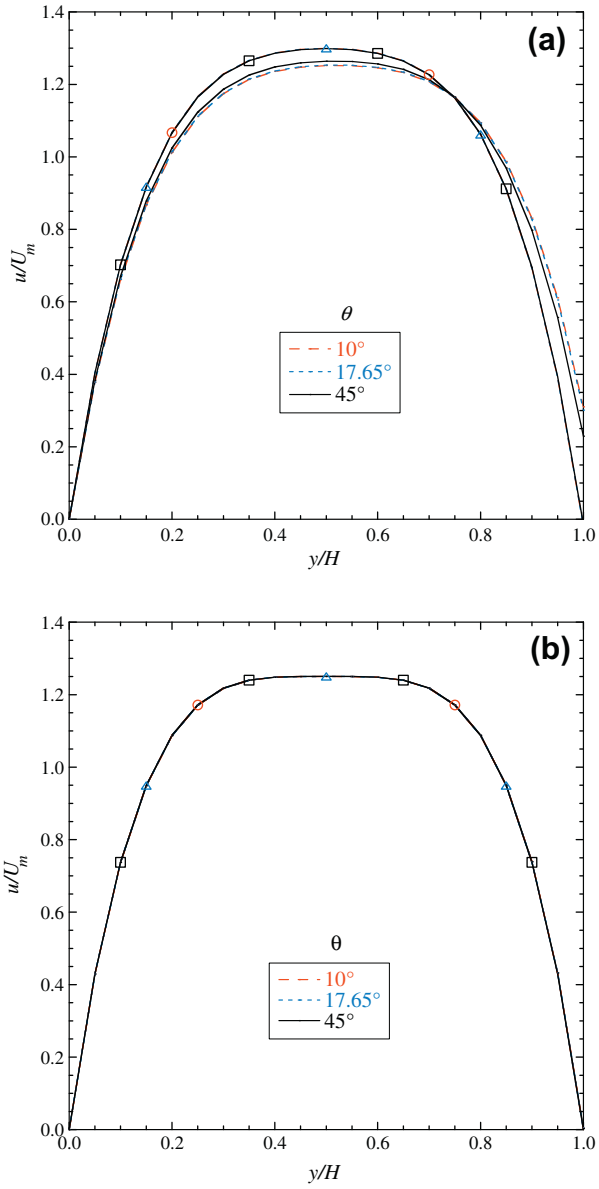

Fig. 6. Transverse profiles of u/U_m as a function of screw angle for $V_p/U_N = -0.1$ (symbols) and $V_p/U_N = 2$ (no symbols): (a) $\varepsilon Wi^2 = 0.1$; (b) $\varepsilon Wi^2 = 10$.

direction increase by a larger fraction than in the main direction, since in the latter the flow is also driven by a pressure gradient, whereas in the former it is only driven by the motion of the plate. When the pressure gradient is adverse as in the screw extruder operation, $-P_{zx} < 0$ and the plot confirms that the variation of $+P_{zx}$ with εWi^2 follows the same trend as for a favorable pressure gradient. Similarly the effect of V_p/U_N upon $|P_{zx}|$ is qualitatively similar regardless of whether the pressure gradient is favorable or adverse.

Similarly, keeping the ratio V_p/U_N fixed and varying the angle of the screw, as in Fig. 3b) increases both the u and w velocity components, but proportionally more the component in the secondary direction (w) than in the main direction (u). What is actually happening, as will become clearer in subsequent figures, is that for increasing levels of shear-thinning the flow in the main direction increases significantly more than in the secondary direction, i.e. there is a large increase in u, which is driven by both the motion of the plate as by the main pressure gradient $\partial p/\partial x$, whereas the flow along z, driven exclusively by the dragging plate, which induces $\partial p/\partial z$, is of the same order of magnitude as for low values of εWi^2.

The above finding is more clearly seen in the plots of Fig. 4. Here, the ratio between the bulk velocity in the main direction (U_m) and the corresponding Newtonian bulk velocity (U_N) is plotted and we observe several important results: (1) the variation of U_m/U_N as a function of εWi^2 is essentially independent of both V_p/U_N (cf. Fig. 4-a) and of θ (cf. Fig. 4-b) (actually, inspection of Eq. (17) shows that the independence of U_m/U_N on both V_p/U_N and θ, is a consequence of the dominant influence of εWi^2 at large values of εWi^2, and this is corroborated by the zoomed view at the inset of Fig. 4a); (2) the increase of U_m/U_N is large resulting in values in excess of 1000 for $\varepsilon Wi^2 \geqslant 23.2$. At the same time the velocities in the secondary direction are of the order of V_p, which is of the order of U_N. This is seen in both Fig. 5a and b, which plot the positive bulk mean velocity in the z-direction $\left(W_m = \int_0^{y@w=0} w dy/H\right)$ as a

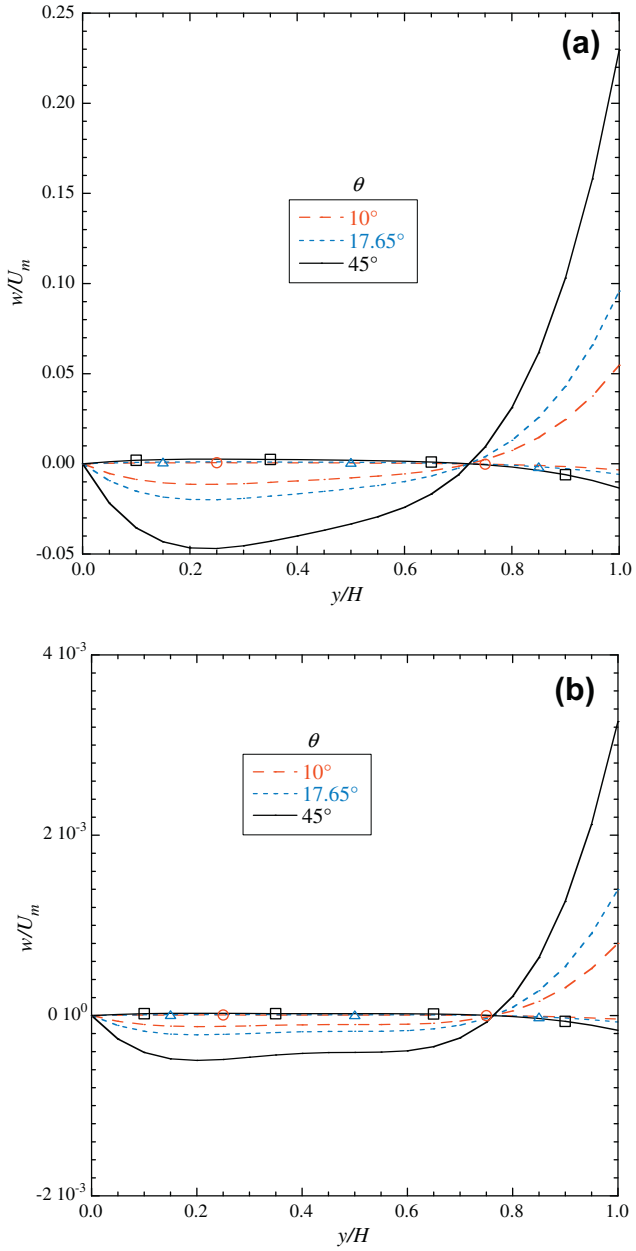

Fig. 7. Transverse profiles of w/U_m as a function of screw angle for $V_p/U_N = -0.1$ (symbols) and $V_p/U_N = 2$ (no symbols): (a) $\varepsilon Wi^2 = 0.1$; (b) $\varepsilon Wi^2 = 10$.

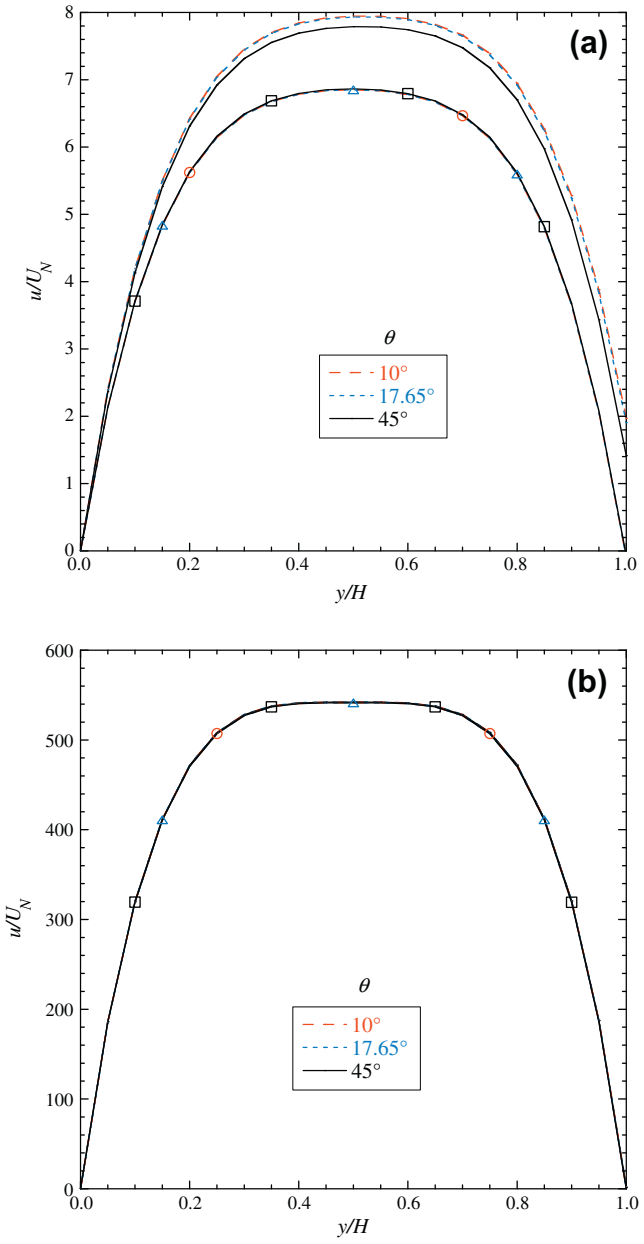

Fig. 8. Transverse profiles of u/U_N as a function of screw angle for $V_p/U_N = -0.1$ (symbols) and $V_p/U_N = 2$ (no symbols): (a) $\varepsilon Wi^2 = 0.1$; (b) $\varepsilon Wi^2 = 10$.

function of the same non-dimensional numbers as in Fig. 4. These figures also show that from a qualitative point of view these findings are independent of whether the flow is occurring under a favorable or an adverse streamwise pressure gradient and the relative position of the various curves essentially depends on the magnitude of $|V_p/U_N|$.

These effects of shear-thinning, with the consequent large increase of the velocity in the main direction, but not in the secondary direction, are also shown in Figs. 6 and 7. Fig. 6a and b plot transverse profiles of the main velocity component as a function of screw angle for low shear-thinning ($\varepsilon Wi^2 = 0.1$) and high shear-thinning ($\varepsilon Wi^2 = 10$) flow conditions, respectively. Since the profiles were made dimensionless by its own bulk velocity the values are similar, with maximum velocities of the order of 1.2 of the bulk velocity and the effect of the screw angle is only visible when the flow in the secondary direction is not too small, i.e., for $\varepsilon Wi^2 = 0.1$. Even though the profiles are all similar, small differences between them are easier to spot for higher values of V_p/U_N and lower values of εWi^2.

The corresponding profiles for the secondary velocity component (w) are plotted in Fig. 7a and b. These are naturally proportional to the magnitude of $|V_p/U_N|$. For Newtonian and weakly shear-thinning fluids with $V_p/U_N = 2$, say $\varepsilon Wi^2 = 0.1$, the values of w/U_m are of the order of 0.1 comparing to values of u/U_m of the order of 1, but for strongly shear-thinning fluids the values of w/U_m are now of the order of 0.001, i.e., one hundred times lower. In agreement with this finding, note also that the wall velocity at $y/H = 1$, corresponding to the velocity of the moving plate, has dropped: it is of the order of 0.25 U_m, but it is so small in Fig. 6b that it looks as though it is null. These values decrease by a factor of about 20 for the profiles pertaining to $V_p/U_N = -0.1$ due to lower wall velocity.

Alternatively, we can plot the same velocity profiles of Figs. 6 and 7 normalized instead by the Newtonian reference velocity,

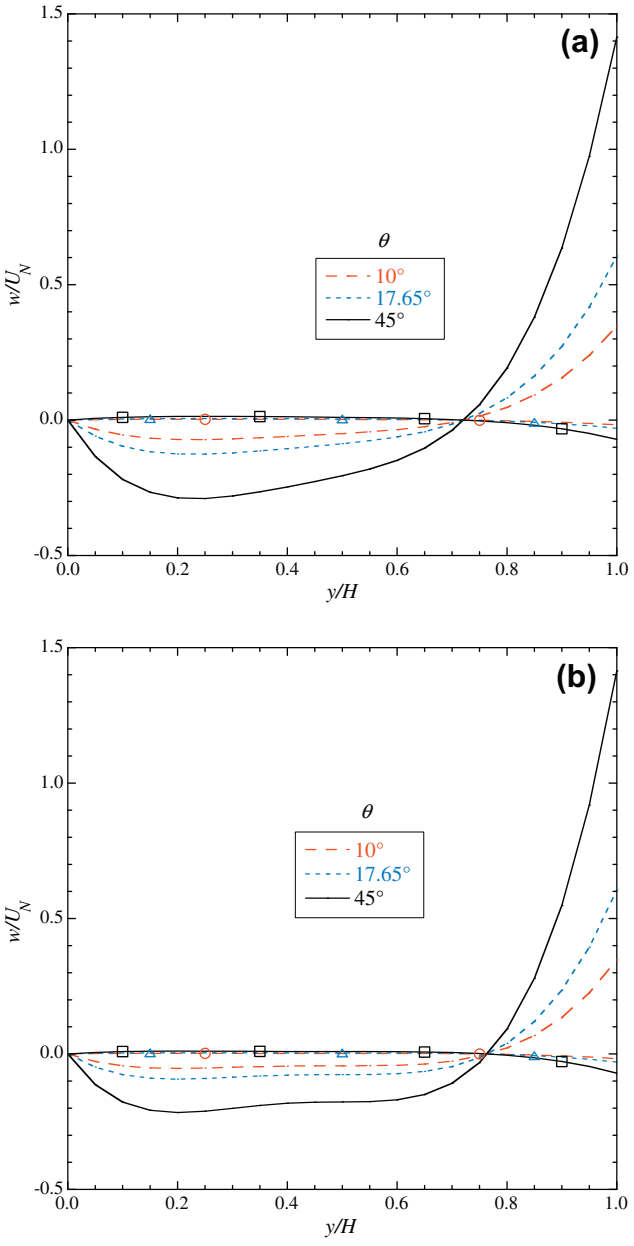

Fig. 9. Transverse profiles of w/U_N as a function of screw angle for $V_p/U_N = -0.1$ (symbols) and $V_p/U_N = 2$ (no symbols): (a) $\varepsilon Wi^2 = 0.1$; (b) $\varepsilon Wi^2 = 10$.

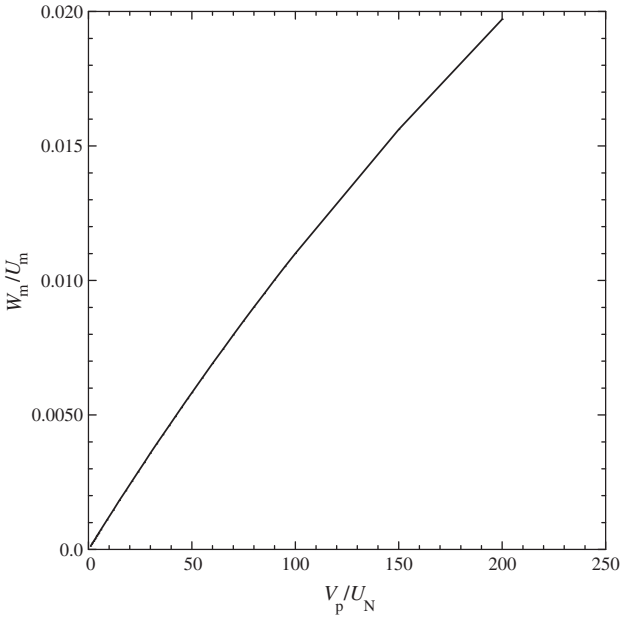

Fig. 10. Variation of W_m/U_m with V_p/U_N for $\varepsilon Wi^2 = 10$ and $\theta = 17.65°$.

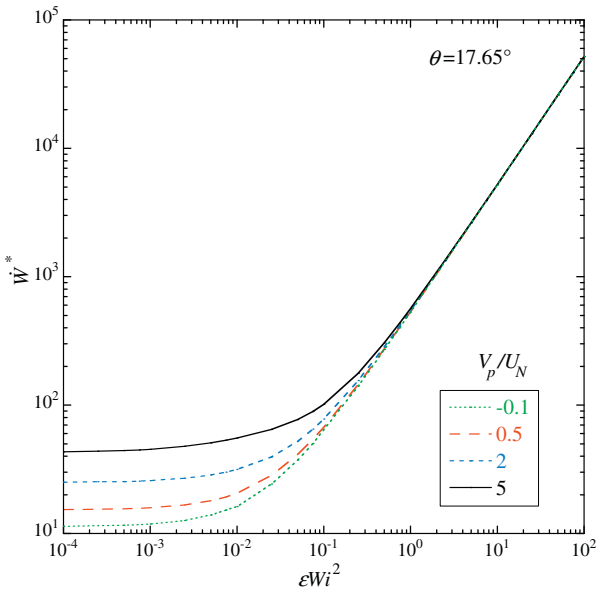

Fig. 11. Variation of $\dot{W}^*$ with εWi^2 and as a function of V_p/U_N for a square extruder ($\theta = 17.65°$).

which is always of the same order of magnitude of the moving plate velocity. These profiles are shown in Figs. 8 and 9 for u/U_N and w/U_N, respectively, all other parameters taking on the same values as in previous figures. In this representation, the secondary velocity profiles are now almost unchanged with εWi^2 and we observe the large increase in the main velocity associated with shear-thinning that allows for much higher streamwise velocities for the same main pressure gradient. The effect of screw angle becomes clearer in the profiles of w, showing that higher angles are always associated with larger velocities in the secondary direction. The profiles for $V_p/U_N = -0.1$ are again about 20 times smaller than those for $V_p/U_N = 2$ and in addition they have the opposite sign because with the adverse pressure gradient U_N is now negative.

From these results it is clear that to create fluid rotation inside the channel with viscoelastic shear-thinning fluids it will be necessary to increase the velocity of the moving plate, which in practical terms is equivalent to an increase in the rotational speed of the screw. However, it can be difficult to achieve values of W_m/U_m of the same order of those found for Newtonian and weakly shear-thinning fluids. As shown in Fig. 10 for $\varepsilon Wi^2 = 10$, the ratio W_m/U_m increases slightly less than linearly with V_p/U_N so that for $V_p/U_N = 200$, W_m/U_m reaches a mere 0.02 for a fixed value of $\varepsilon Wi^2 = 10$ and a screw angle of 17.65° (corresponding to the square screw). In practical terms this is not such a severe limitation because such a high value of εWi^2 may not be reached due to other effects as the appearance of flow instabilities at the die exit [27], which impose a limit to the throughput.

The variation of power with shear-thinning, with V_p/U_N as a parameter, is exhibited in Fig. 11. For Newtonian and weakly shear-thinning fluids the normalized dissipated power of Eq. (22) is independent of εWi^2 but increases with V_p/U_N by a factor of

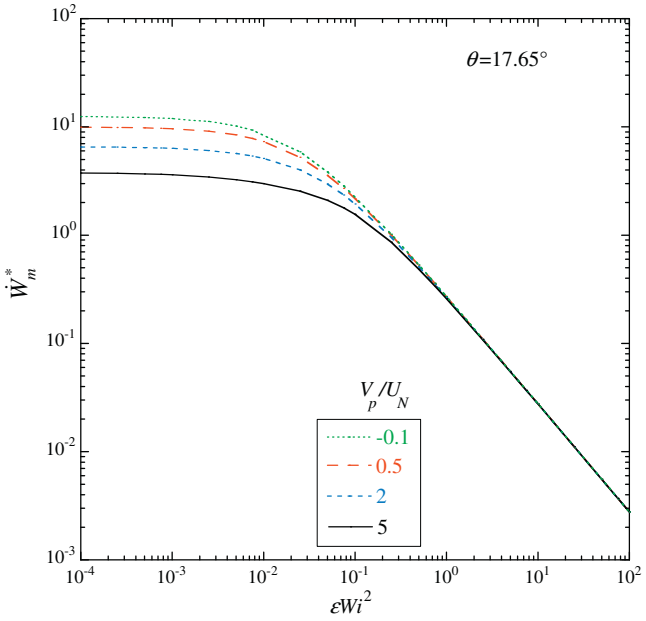

Fig. 12. Variation of the renormalized power $\left(\dot{W}^*_m \equiv \dot{W}^* U_N^2/U_m^2\right)$ with εWi^2 and as a function of V_p/U_N for a square extruder ($\theta = 17.65°$).

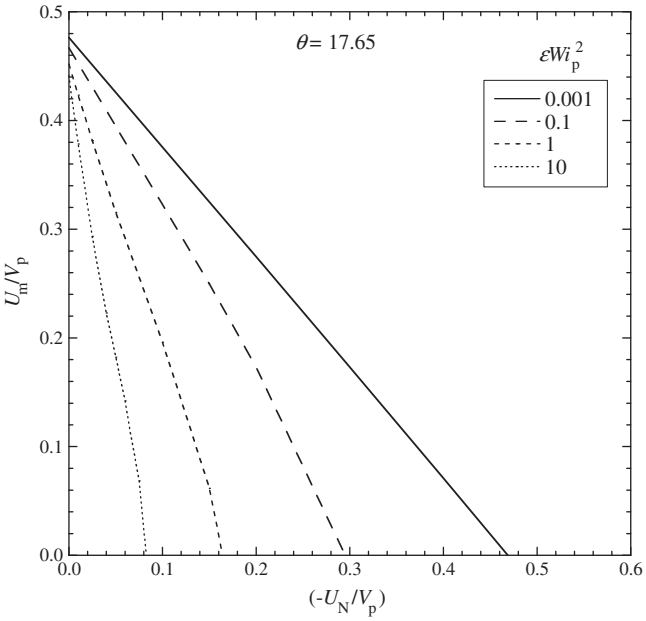

Fig. 13. Variation of the dimensionless flow rate as a function of dimensionless pressure rise through a screw extruder pump as a function of εWi_p^2 for a square screw ($\theta = 17.65°$).

around 2.6 when this parameter increases 10 times, from 0.5 to 5. Then, as εWi^2 grows above 1 the normalized power becomes independent of V_p/U_N, while increasing exponentially with εWi^2 (this corresponds to a linear variation on the log-log scale of Fig. 11). These large values of $\dot{W}^*$ are due to the normalization by the characteristic velocity of the pressure gradient, U_N, which is much smaller than the streamwise bulk velocity at large values of εWi^2 (it is only identical at $\varepsilon Wi^2 = 0$). By renormalizing the power with U_m, leading to $\dot{W}^*_m \equiv \dot{W}^*\left(U_N^2/U_m^2\right)$, the opposite effect is observed as shown in Fig. 12. As εWi^2 increases the fluid becomes more shear-thinning and the apparent viscosity decreases so that the same flow rate is imposed by a smaller pressure gradient, therefore the power dissipated per unit flow rate decreases. Finally, Fig. 13 shows the characteristic curve for a pumping square screw in dimensionless form with εWi^2 as a parameter. The normalized pressure rise for a given flow rate is seen to decrease, because of the reduction in viscosity associated with shear-thinning.

5. Final remarks

We obtained an analytical solution for the isothermal flow of viscoelastic fluids in a single-screw extruder under the simplified classical conditions of a shallow stationary two-dimensional screw and a moving barrel, thus defining two Couette–Poiseuille flows, one of which is characterized by a null flow rate. Both elementary flows were considered to depend only on the transverse coordinate, i.e., the effects of the spanwise coordinate were neglected to allow a simple analytical solution as is typical in shallow extruders. The viscoelastic model is the simplified Phan-Thien—Tanner constitutive equation with the linear kernel function of the trace of the stress tensor. The nonlinear nature of this constitutive equation couples both Couette–Poiseuille flows and invalidates the superposition principle.

The results show that for $\varepsilon Wi^2 \leqslant 0.01$, i.e., for weakly elastic flow conditions, the flow is little affected by the non-Newtonian characteristics and the Newtonian solution is essentially recovered and that for $\varepsilon Wi^2 \geqslant 0.1$ the pressure gradient ratio varies in inverse proportion to εWi^2 in a log-law scale, essentially because the streamwise flow becomes progressively more affected by the shear-thinning of the viscosity, whereas the secondary flow imposed by the moving barrel remains very much unchanged. Hence, the streamwise flow rate increases strongly with εWi^2 while the secondary flow just rearranges. This can be partially offset by increasing the angle of the helix. The characteristic curve of the pumping screw extruder is also presented in dimensionless form showing the reduction of the pressure rise associated with an increase in εWi^2.

Future work may possibly consider the variation of the boundary condition at the flight with the channel thickness, which requires the treatment of this flow with stationary barrel and a moving screw.

Acknowledgements

D.O.A. Cruz gratefully acknowledges the sabbatical leave of absence from Universidade Federal do Pará and the funding by CNPq (200120/2009-3). FT Pinho acknowledges support by CEFT and facilities provided by Departamento de Engenharia Mecânica at FEUP to accommodate Prof. D.O.A. Cruz during his stay in Portugal.

Appendix A

As explained at the end of Section 3, for the purpose of analyzing the pumping by the screw extruder it is more convenient to normalize the derived solution using as a velocity scale the plate velocity V_p instead of the velocity scale U_N. The main equations of the derived solution are written below with this new normalization and the rules of transformation between the normalization with U_N and with V_p are given in Eq. (A.1).

$$T^*_{xy_0} = T_{xy_0}\frac{U_N}{V_p}, \quad T^*_{zy_0} = T_{zy_0}\frac{U_N}{V_p}, \quad Wi_p = Wi\frac{V_p}{U_N} \text{ and}$$
$$P_{zx} = \frac{U_z}{U_N}. \tag{A.1}$$

Now, the relationships between the normal and shear stresses are

$$T^*_{xx} = 12Wi_pT^{*2}_{xy},$$
$$T^*_{zz} = 12Wi_pT^{*2}_{zy}, \tag{A.2-a, b}$$

and the profiles of shear stress across the channel are given by

$$T^*_{xy} = -2\frac{y}{H}\frac{U_N}{V_p} + T^*_{xy_0},$$
$$T^*_{zy} = -2\frac{y}{H}\frac{U_z}{V_p} + T^*_{zy_0}. \quad \text{(A.3-a, b)}$$

The profiles of the velocity components are given by Eq. (A.4-a,b).

$$\frac{u}{V_p} = -6\frac{y}{H}\left\{48\varepsilon Wi_p^2\left(\frac{U_z}{V_p}\right)^2\left(\frac{y}{H}\right)^2\left[3\frac{y}{H}\frac{U_N}{V_p} - 2T^*_{xy_0}\right]\right.$$
$$- 48\varepsilon Wi_p^2\frac{U_z}{V_p}\frac{y}{H}\left[4\frac{y}{H}\frac{U_N}{V_p} - 3T^*_{xy_0}\right]T^*_{zy_0}$$
$$+ \left[\frac{y}{H}\frac{U_N}{V_p} - T^*_{xy_0}\right]\left[1 + 144\varepsilon Wi_p^2\left(\frac{U_N}{V_p}\right)^2\left(\frac{y}{H}\right)^2\right.$$
$$\left.\left. + 72\varepsilon Wi_p^2\left[-2\frac{y}{H}\frac{U_N}{V_p}T^*_{xy_0} + T^{*2}_{xy_0} + T^{*2}_{zy_0}\right]\right]\right\},$$
$$\frac{w}{V_p} = -6\frac{y}{H}\left\{144\varepsilon Wi_p^2\left(\frac{U_N}{V_p}\right)^2\left(\frac{U_z}{V_p}\right)\left(\frac{y}{H}\right)^3\left[1 + \frac{(U_z/V_p)^2}{(U_N/V_p)^2}\right]\right.$$
$$-96\varepsilon Wi_p^2\left(\frac{y}{H}\right)^2\left[2\frac{U_N}{V_p}\frac{U_z}{V_p}T^*_{xy_0} + \left(\frac{U_N}{V_p}\right)^2 T^*_{zy_0} + 3\left(\frac{U_z}{V_p}\right)^2\frac{U_z/V_p}{U_N/V_p}T^*_{zy_0}\right]$$
$$-T^*_{zy_0}\left[1 + 72\varepsilon Wi_p^2\left(T^{*2}_{xy_0} + T^{*2}_{zy_0}\right)\right] + \frac{y}{H}\frac{U_N}{V_p}\left[144\varepsilon Wi_p^2 T^*_{xy_0}T^*_{zy_0}\right.$$
$$\left.\left. + \frac{U_z/V_p}{U_N/V_p}\left[1 + 72\varepsilon Wi_p^2\left(T^{*2}_{xy_0} + 3T^{*2}_{zy_0}\right)\right]\right]\right\}. \quad \text{(A.4-a, b)}$$

As for the solution in the main text, these profiles depend on the velocity boundary conditions at the top wall ($u/V_p = \cos\theta$ and $w/V_p = \sin\theta$ at $y/H = 1$), which provide the wall shear stresses $T^*_{xy_0}$ and $T^*_{zy_0}$ and on the condition of null flow rate in the z-direction ($\overline{W} = 0$) to quantify the corresponding pressure gradient ($p_{,z}$) via its dimensionless form U_z/V_p. These three quantities are calculated numerically from the following set of three nonlinear algebraic equations

$$-6\left\{48\varepsilon Wi_p^2\left(\frac{U_z}{V_p}\right)^2\left(3\frac{U_N}{V_p} - 2T^*_{zy_0}\right)\right.$$
$$-48\varepsilon Wi_p^2\left(\frac{U_z}{V_p}\right)T^*_{zy_0}\left(4\frac{U_N}{V_p} - 3T^*_{xy_0}\right) + \left(\frac{U_N}{V_p} - T^*_{xy_0}\right)$$
$$\left.\times\left[1 + 144\varepsilon Wi_p^2\left(\frac{U_N}{V_p}\right)^2 + 72\varepsilon Wi_p^2\left(T^{*2}_{xy_0} - 2\frac{U_N}{V_p}T^*_{xy_0} + T^{*2}_{zy_0}\right)\right]\right\} = \cos\theta, \quad \text{(A.5-a)}$$

$$-6\left\{144\varepsilon Wi_p^2\frac{U_N}{V_p}\frac{U_z}{V_p}\left(\frac{U_N}{V_p} + \frac{(U_z/V_p)^2}{(U_N/V_p)}\right) + 144\varepsilon Wi_p^2\frac{U_N}{V_p}T^*_{xy_0}T^*_{zy_0}\right.$$
$$-96\varepsilon Wi_p^2\left(2\frac{U_z}{V_p}\frac{U_N}{V_p}T^*_{xy_0} + \left(\frac{U_N}{V_p}\right)^2 T^*_{zy_0} + 3\left(\frac{U_z}{V_p}\right)^2 T^*_{zy_0}\right)$$
$$-T^*_{zy_0}\left[1 + 72\varepsilon Wi_p^2\left(T^{*2}_{xy_0} + T^{*2}_{zy_0}\right)\right]$$
$$\left.+\frac{U_z}{V_p}\left[1 + 72\varepsilon Wi_p^2\left(T^{*2}_{xy_0} + 3T^{*2}_{zy_0}\right)\right]\right\} = \sin\theta, \quad \text{(A.5-b)}$$

$$-\frac{2}{5}\frac{U_z}{V_p}\left\{5 + 432\varepsilon Wi_p^2\left(\frac{U_N}{V_p}\right)^2 + 72\varepsilon Wi_p^2\left[6\left(\frac{U_z}{V_p}\right)^2\right.\right.$$
$$\left.\left.+5T^*_{xy_0}\left(T^*_{xy_0} - 2\frac{U_N}{V_p}\right)\right]\right\} + 3T^*_{zy_0} + 72\varepsilon Wi_p^2 T^*_{zy_0}\left[2\left(\frac{U_N}{V_p}\right)^2\right.$$
$$\left.+6\left(\frac{U_z}{V_p}\right)^2 + T^*_{xy_0}\left(3T^*_{xy_0} - 4\frac{U_N}{V_p}\right)\right] + 216\varepsilon Wi_p^2 T^{*2}_{zy_0}\left(T^*_{zy_0} - 2\frac{U_N}{V_p}\right) = 0. \quad \text{(A.5-c)}$$

The streamwise bulk velocity is given by Eq. (A.6)

$$\frac{U_m}{V_p} = -2\frac{U_N}{V_p} + 3T^*_{xy_0} + \frac{72}{5}\varepsilon Wi_p^2\left\{-12\left(\frac{U_N}{V_p}\right)^3 + 2\left(\frac{U_z}{V_p}\right)^2\left(5T^*_{xy_0} - 6\frac{U_N}{V_p}\right)\right.$$
$$- 20\frac{U_z}{V_p}\left(T^*_{xy_0} - \frac{U_N}{V_p}\right)T^*_{zy_0} - 10\frac{U_N}{V_p}T^{*2}_{xy_0} + 15T^*_{xy_0}\left[2\left(\frac{U_N}{V_p}\right)^2\right.$$
$$\left.\left. + \left(T^*_{xy_0} - 2\frac{U_N}{V_p}\right)T^*_{xy_0} + T^{*2}_{xy_0}\right]\right\}, \quad \text{(A.6)}$$

and the power dissipated by friction per unit area is now given by Eq. (A.7)

$$\dot{W}^* = \frac{\dot{W}/(WL)}{\eta V_p^2/H}$$
$$= 12\frac{U_m}{V_p}\frac{U_N}{V_p} + \left[\cos\theta\left(2\frac{U_N}{V_p} - T^*_{xy_0}\right) + \sin\theta\left(-2\frac{U_z}{V_p} + T^*_{zy_0}\right)\right]. \quad \text{(A.7)}$$

References

[1] Z. Tadmor, I. Klein, Engineering Principles of Plasticating Extrusion, Van Nostrand Reynolds, New York, 1970.
[2] Z. Tadmor, C.G. Gogos, Principles of Polymer Processing, second ed., Wiley Interscience, Hoboken, 2006.
[3] H.F. Giles Jr., J.R. Wagner Jr., E.M. Mount III, Extrusion: The Definitive Processing Guide and Handbook, William Andrew, Norwich, NY, USA, 2005.
[4] C. Rauwendaal, Polymer Extrusion, fourth ed., Hanser Verlag, Munich, 2001.
[5] J.-F. Agassant, P. Avenas, J.-Ph. Sergent, P.J. Carreau, Polymer Processing, in: Principles and Modelling, Hanser Publishers, Munich, 1991.
[6] R.K. Shah, A.L. London, Laminar Flow Forced Convection in Ducts, Academic Press, London, 1978.
[7] H.L. Dryden, F.D. Murnaghan, H. Bateman, Hydrodynamics Bull. No. 84, pp. 197–201, Comm. Hydrodyn., Div. Phys. Sci., Natl. Res. Council, Washington, DC, 1932 (reprinted by Dover, New York, 1956).
[8] S.M. Marco, L.S. Han, A note on limiting laminar Nusselt number in ducts with constant temperature gradient by analogy to thin-plate theory, Trans. ASME 77 (1955) 625–630.
[9] V. Theofilis, P.W. Duck, J. Owen, Viscous linear stability analysis of rectangular duct and cavity flows, J. Fluid Mech. 505 (2004) 249–286.
[10] F.M. White, Viscous Fluid Flow, second ed., McGraw-Hill, New York, 1991.
[11] Y. Li, F. Hsieh, Modeling of flow in a single screw extruder, J. Food Eng. 27 (1996) 353–375.
[12] K.P. Choo, N.R. Neelakantan, J.F.T. Pittman, Experimental deep channel velocity profiles and operating characteristics for a single-screw extruder, Pol. Eng. Sci. 20 (1980) 349–356.
[13] K.L. McCarthy, R.J. Kanten, C.K. Agemura, Application of NMR imaging to the study of velocity profiles during extrusion processing, Trends Food Sci. Technol. 3 (1992) 215–219.
[14] N. Phan-Thien, R.I. Tanner, A new constitutive equation derived from network theory, J. Non-Newt. Fluid Mech. 2 (1977) 353–365.
[15] H. Giesekus, A simple constitutive equation for polymer fluids based on the concept of deformation-dependent tensorial mobility, J. Non-Newt. Fluid Mech. 11 (1982) 69–109.
[16] A.I. Leonov, Nonequilibrium thermodynamics and rheology of viscoelastic polymer media, Rheol. Acta 15 (1976) 85–98.
[17] T.C.B. McLeish, R.G. Larson, Molecular constitutive equations for a class of branched polymers: The pom–pom polymer, J. Rheology. 42 (1998) 81–110.
[18] R.G. Larson, The Structure and Rheology of Complex Fluids, Oxford University Press, Oxford, 1999.
[19] J.A. Wheeler, E.H. Wissler, Steady flow of non-Newtonian fluids in a square duct, Trans. Soc. Rheol. 10 (1966) 353–367.
[20] J.P. Hartnett, M. Kostic, Heat transfer to a viscoelastic fluid in laminar flow through a rectangular channel, Int. J. Heat Mass Transfer 28 (1985) 1147–1155.
[21] N. Peres, A.M. Afonso, M.A. Alves, F.T. Pinho, Heat transfer enhancement in laminar flow of viscoelastic fluids through a rectangular duct. Paper 551.pdf in Congreso de Métodos Numéricos en Ingeniería 2009, Barcelona, 29th June–2nd July, 2009.
[22] P. Yue, J. Dooley, J.J. Feng, A general criterion for viscoelastic secondary flow in pipes of noncircular cross section, J. Rheol. 52 (2008) 315–332.
[23] S.Y. Poon, The flow of a power law fluid in a melt-fed single-screw extruder, ASME J. Fluids Eng. 95 (1973) 81–90.
[24] D. Gabriele, S. Curcio, B. de Cindio, Optimal design of single-screw extruder for liquorice candy production: a rheology based approach, J. Fluids Eng. 48 (2001) 33–44.
[25] J.D. Guzmán, J.D. Schieber, Analysis of closed-discharge single-screw extrusion of power-law fluids, Polym. Eng. Sci. 43 (2003) 55–61.
[26] R. Chella, J.M. Ottino, Fluid mechanics of mixing in a single-screw extruder, Ind. Eng. Chem. Fundam. 24 (1985) 170–180.
[27] M.M. Denn, Extrusion instabilities and wall slip, Ann. Rev. Fluid Mech. 33 (2001) 265–287.